Mitochondrial adaptation decreases drug sensitivity of persistent triple negative breast cancer cells surviving combinatory and sequential chemotherapy

Marie Winter, Amina Nait Eldjoudi, Catherine Guette, Hubert Hondermarck, Roland Bourette, Quentin Fovez, William Laine, Bart Ghesquiere, Eric Adriaenssens, Jérôme Kluza, et al.

Neoplasia 46 (2023) 100949

Contents lists available at ScienceDirect

Neoplasia

journal homepage: www.elsevier.com/locate/neo

Original Research

Mitochondrial adaptation decreases drug sensitivity of persistent triple negative breast cancer cells surviving combinatory and sequential chemotherapy

Marie Winter [a,1], Amina Nait Eldjoudi [a,1], Catherine Guette [b], Hubert Hondermarck [c,d], Roland P. Bourette [a], Quentin Fovez [a], William Laine [a], Bart Ghesquiere [e,f], Eric Adriaenssens [a], Jérôme Kluza [a,2], Xuefen Le Bourhis [a,2,*]

[a] UMR9020—U1277-CANTHER—Cancer Heterogeneity, Plasticity and Resistance to Therapies, University of Lille, CNRS, Inserm, CHU Lille, F-59000 Lille, France
[b] ICO, Inserm, CNRS, Nantes Université, CRCI2NA, Université d'Angers, Angers, France
[c] School of Biomedical Sciences and Pharmacy, College of Health, Medicine and Wellbeing, University of Newcastle, Callaghan, NSW2308, Australia
[d] Hunter Medical Research Institute, University of Newcastle, New Lambton Heights, NSW2305, Australia
[e] Metabolomics Expertise Center, Center for Cancer Biology, CCB-VIB, VIB, Leuven, 3000, Belgium
[f] Metabolomics Expertise Center, Department of Oncology, KU Leuven, Leuven, 3000, Belgium

ARTICLE INFO

Keywords:
Persistence
Resistance
Chemotherapy
Mitochondrial adaptation
Pyruvate

ABSTRACT

Triple negative breast cancer (TNBC) is an aggressive malignancy for which chemotherapy remains the standard treatment. However, between 3 and 5 years after chemotherapy, about half patients will relapse and it is essential to identify vulnerabilities of cancer cells surviving neoadujuvant therapy. In this study, we established persistent TNBC cell models after treating MDA-MB-231 and SUM159-PT TNBC cell lines with epirubicin and cyclophosphamide, and then with paclitaxel, for a total of 18 weeks. The resulting chemo-persistent cell lines were more proliferative, both *in vitro* and in xenografted mice. Interestingly, MDA-MB-231 persistent cells became less sensitive to chemotherapeutic drugs, whereas SUM159-PT persistent cells kept similar sensitivity compared to control cells. The reduced sensitivity to chemotherapy in MDA-MB-231 persistent cells was found to be associated with an increased oxidative phosphorylation (OXPHOS) and modified levels of tricarboxylic acid cycle (TCA) intermediates. Integration of data from proteomics and metabolomics demonstrated TCA cycle among the most upregulated pathways in MDA-MB-231 persistent cells. The absence of glucose and pyruvate impeded OXPHOS in persistent cells, while the absence of glutamine did not. In contrast, OXPHOS was not modified in control cells independently of TCA substrates, indicating that MDA-MB-231 persistent cells evolved towards a more pyruvate dependent profile. Finally, the inhibition of pyruvate entry into mitochondria with UK-5099 reduced OXPHOS and re-sensitized persistent cells to therapeutic agents. Together, these findings suggest that targeting mitochondrial pyruvate metabolism may help to overcome mitochondrial adaptation of chemo-persistent TNBC.

Introduction

Triple negative breast cancer (TNBC) represents 15-20 % of all breast cancers and is defined by the lack of estrogen receptor, progesterone receptor and human epidermal growth factor receptor 2 [1]. Development of targeted drugs in TNBC is challenging since classic protein tyrosine kinase inhibitors fail to have the same efficacy in TNBC patients compared to other cancers. The PARP1 inhibitors olaparib and talazoparib, the PD-L1 inhibitor atezolizumab, and the antibody-drug conjugate sacituzumab-govitecan have been recently used, but they are unable to fully satisfy the clinical requirement for patients with TNBC [2]. So far, only a minority of patients have benefited from these emerging targeted treatments, and chemotherapy remains the current standard of care. TNBC displays about 2-fold pathological complete

* Corresponding author.
E-mail address: xuefen.le-bourhis@univ-lille.fr (X. Le Bourhis).
[1] These authors have contributed equally to this work.
[2] The two last authors have contributed equally to this work.

https://doi.org/10.1016/j.neo.2023.100949
Received 21 July 2023; Received in revised form 30 October 2023; Accepted 30 October 2023
Available online 11 November 2023

response (pCR) rate to chemotherapy when compared to other breast cancer subtypes [3–5]. However, more than 30 % of TNBC relapse within 3 years of treatment and about half of TNBC patients treated with neoadjuvant chemotherapy present substantial residual cancer burden [6–8]. Relapsed and metastatic TNBCs is usually more aggressive, showing strong resistance to chemo- and radiotherapies with a median patient overall survival (OS) of about 18 months [9]. Various molecular mechanisms underlying TNBC therapeutic resistance and disease recurrence have been reported. These include increased drug efflux and metabolism, enhanced antioxidant and DNA repair abilites, up-regulation of the pro-survival proteins Mcl-1 and Bcl-2, epithelial-mesenchymal transition (EMT), reprogramming of cancer non stem cells into cancer stem cells, and metabolic reprogramming [2]. Also, TNBC stem-like cells have been shown to display chemoresistance and increased OXPHOS activity [10].

Metabolic reprogramming, also known as the Warburg effect refers to the preference of cancer cells to metabolize glucose thorough glycolysis, even under normoxia, which contributes to chemoresistance. The enhanced aerobic glycolysis permits energy production and the synthesis of nucleotides, amino acids and lipids, which are essential for tumor growth and progression, especially under the survival pressures such as hypoxia, anoikis, as well as radio- and chemo-therapy-induced DNA damages [11]. Increased glycolysis can favour chemoresistance through several mechanisms. For example, the non-oxidative pentose phosphate pathway (PPP) has been reported to protect TNBC cells from chemotherapeutic drugs-induced DNA damage through increased nucleotide metabolism [12]. Doxorubicin-resistant TNBC cells have been shown to overexpress the PPP rate-limiting enzyme glucose-6-phosphate dehydrogenase (G6PD), leading to the production of nicotinamide adenine dinucleotid phosphate (NADPH) and the increased synthesis of the antioxidant glutathione, which in turn reduces chemotherapy-induced ROS and DNA damage [13]. Increased glycolysis also favors the accumulation of H+ in the cytoplasm, leading to reduced influx of alkaline drugs such as doxorubicin [14]. However, in contrast with clinical practice, the majority of fundamental studies have been performed with only one chemotherapeutic drug. Moreover, most experiments were performed immediately after short-term drug treatment or after chronic treatment with drug concentrations too much high compared to that used in clinics [15–17]. Few studies investigated the phenotypic and metabolic adaptations of TNBC cells after a long-term combined and sequential chemotherapeutic treatment. The aim of this study is to generate a relevant chemotherapy persistent cellular model mimicking clinical neoadjuvant treatment, and to unveil molecular and metabolic modifications in triple negative breast cancer cells surviving combinatory and sequential chemotherapy.

Materials and methods

Cell culture

MDA-MB-231 TNBC cell line (from ATCC) was maintained in MEM (Minimal Essential Medium, Life technologies, Villebon-sur-Yvette, France) supplemented with 10 % inactivated FCS (Fœtal Calf Serum) (Sigma, Saint-Quentin-Fallavier, France), 1 % non-essential amino acid, 40 UI/mL penicillin, 40 μg/mL streptomycin (Biovalley, Nanterre, France) at 37°C in 5 % CO_2-humidified atmosphere. SUM159-PT TNBC cell line (from Asterand Bioscience, Detroit, MI, USA) was cultured in Ham's F12 culture medium supplemented with 5 % FCS, 10 mM HEPES, 5 μg/mL insulin, 1 μg/mL hydrocortisone (Sigma, Saint-Quentin-Fallavier,France), 1 % ZellShield (Minerva biolabs, Berlin, Germany) at 37°C in 5 % CO_2-humidified atmosphere.

Generation of chemo-persistent cells

To mimic clinical neoadjuvant treatment protocol, MDA-MB-231 and SUM159-PT TNBC cells were first treated with epirubicin and cyclophosphamide (Selleckchem, Planegg, Germany), with a clinically used ratio of 1:5 for 3 cycles. Each cycle lasted for 3 weeks: 2 days of treatment in culture medium containing 2 % of FCS allowing for 50 % cell growth inhibition (8 nM epirubicin and 40 nM cyclophosphamide for MDA-MB-231 cells, 40 nM epirubicin and 200 nM cyclophosphamide for SUM159-PT cells) and 19 days of recovery. Then, cells were treated with paclitaxel (Selleckchem, Planegg, Germany) for 9 cycles. Each cycle lasted for 1 week: 2 days of treatment (1 nM paclitaxel for MDA-MB-231 cells or 2 nM paclitaxel for SUM159-PT cells) allowing for 50 % cell growth inhibition and 5 days of recovery. In parallel, control cells were maintained in drug free medium supplemented with 2 % of FCS. The resulting persistent and control cells, were amplified and cryoconserved in liquid nitrogen for further analysis.

Cell growth assays

Cell growth assay in 2D culture

Cells were seeded in 6-well plates (50,000 cells/well) (Falcon; Fisher Scientific, Illkirch-graffenstaden, France) and cultured for 4 days in serum free culture media. The number of viable cells was determined using a hemocytometer after incubation with trypan blue for 30 min.

Clonogenic assay

One thousand control or persistent cells were seeded in 6-well plates in culture media containing 10 % FCS (for MDA-MB-231) or 5 % FCS (for SUM159-PT). After 10 days of culture, colonies were stained with crystal violet before counting as previously described [18].

Cell growth assay in 3D Matrigel culture

Cells were harvested and resuspended in MEM or F12 media containing 1 % FCS. Cells suspension (100 cells in 50 μL) was then mixed with 50 μL of growth factor-reduced Matrigel (Corning, Borre, France) to form a droplet. The droplet was deposited in a well of 6-well plates and incubated for 30 min at 37°C, in 5 % CO_2-humidified atmosphere. The droplet was then incubated in culture medium containing 10 % FCS for 10 days, with culture medium replaced 5 days later. At the end of culture, cells were dissociated from Matrigel with 1 mL dispase 1 U (STEMCELL Technologies) and centrifugated (300 *g*, 5 min) to remove Matrigel. Cells were resuspended in culture medium and counted with a hemocytometer.

Cell response to drug treatment

Cell reponse to combined and sequential chemotherapeutic treatment

Control or persistent cells were seeded in 96-well plates (1,000 cells/well) (Falcon) and cultured for 24 h. Cells were first treated with epirubicin and cyclophosphamide for 48 h, and then with paclitaxel for another 48 h. At the end of the treatment, cells are fixed with cold 70 % ethanol and stained with 1 mM Hoechst 33258 during 30 min at room temperature under obscurity. Cell number in each condition was then determined with Celigo (Nexcelcom).

Cell reponse to single drug treatment

Cells were seeded in 96-well plates (1,000 cells/well) (Falcon) and cultured for 24 h. Cells were then treated with different concentrations of epirubicin or paclitaxel for 96 h, fixed with cold 70 % ethanol and stained with 1 mM Hoechst 33258 during 30 min at room temperature under obscurity. Cell number was determined with Celigo.

Co-treatment of OXPHOS inhibitors with chemotherapy drugs

MDA-MB-231 control and persistent cells were seeded in 96-well plates (1,000 cells /well) (Falcon) and cultured for 24 h. Cells were then co-treated with tigecycline or UK-5099 and different concentrations of epirubicin for 96 h. Alternatively, cells were co-treated with tigecycline or UK-5099 and combined chemotherapeutic drugs (epirubicin and cyclophosphamide for the first 48 h and then paclitaxel for

another 48 h). At the end of the treatment, the remaining cells were fixed with cold 70 % ethanol and stained with 1 mM Hoechst 33258 during 30 min at room temperature under obscurity. Cell number was determined with Celigo.

Determination of IC50 and drug synergism

The IC50 of epirubicin and paclitaxel in control or persistent cells was determined by non-linear regression with Graphpad Prism (v 9.1). The drug synergism of tigecycline or UK-5099 with epirubicin was determined with "SynergyFinder" package in R software [19]. The Bliss synergy score was used to determinate: synergistic (=]20; infinity[), additive ([20; -20[) or antagonist effects ([-20; infinity[).

Tumor xenograft growth in SCID mice and primary culture of cancer cells derived from xenografted tumors

MDA-MB-231 control or persistent cells (2×10^6) were subcutaneously injected into the flanks of six-week-old female SCID mice, purchased from Pasteur Institute of Lille (Lille, France) and maintained in accordance with the Institutional Animal Care and Use Committee procedures and guidelines. Tumor volume was determined every 3 days throughout the experiment by measuring the length and width and was calculated as follows: $\pi/6$ x width $\times$ length $\times$ (width + length)/2. At the time of sacrifice, the primary tumor was removed and fragmented into pieces of 1 mm and then the cells were dissociated by enzymatic and mechanic action with the tumor dissociation kit (Miltenyi Biotec 130-095-929) and the gentle MACS dissociator machine following manufacturer's instructions. The dissociated cells were cultured in MEM medium supplemented with FCS 2 % until the measurement of OXPHOS.

Oxygen consumption rate (OCR) and extracellular acidification rate (ECAR) measurement

Extracellular acidification rate measurements (ECAR) and oxygen consumption rate (OCR) were measured using the XFe24 Seahorse analyzer (Seahorse Bioscience, Billerica, MA, USA) as previously published [20]. Briefly, cells were suspended in DMEM (Merck, Darmstadt, Germany) with L-glutamine (2 mM) and NaCl (32 mM) for glycolysis, or L-glutamine (2 mM), glucose (10 mM) and pyruvate (1 mM) for oxygen consumption and seeded at 1×10^5 cells•100 μL^{-1}•well^{-1}. Each port was loaded with 75 µL (XFe24) of inhibitor diluted in OXPHOS medium. The OCR was assessed at baseline and after injection of each of the following molecules: oligomycin A (1µM), FCCP (1.1 and 2.3µM), rotenone and antimycin A (1µM each). To assess the contribution of pyruvate metabolism in OCR, cells were treated with 10 μM UK-5099 (Sigma) 30 min before Seahorse measurements. Spare respiratory capacity (SRC) was calculated as the difference between the maximum rate of mitochondrial respiration and the basal rate of oxygen consumption.

Metabolomic analysis

MDA-MB-231 control and persistent cells were seeded at 25,000 cells/cm^2 in 6-well plates (Falcon) and cultured for 24 h in DMEM containing 5 mM glucose (Life technologie) and 2 mM L-glutamine (Sigma). Cells were rinsed with ice-cold 0.9 % NaCl solution and metabolites were extracted by adding 250 µL of a 50/30/20 solution (methanol-acetonitrile 10 mM Tris-HCl pH 9.4) to the cells. Plates were then incubated for 3 min on ice. Cells were transferred to an Eppendorf tube before centrifugation at 20, 000 g for 10 min at 4°C. Supernatants were then transferred to a fresh tube and stored at -80°C, and pellets were used for BCA/protein assay to normalize each condition to the same cell number. Separation of metabolites prior to Mass Spectrometry (MS) measurement was performed using a Dionex UltiMate 3000 LC System (Thermo Scientific) coupled to a Q Exactive Orbitrap mass spectrometer (Thermo Scientific) operating in negative ion mode.

Proteomic analysis

MDA-MB-231 control and persistent cells (10^6) were seeded in 100 mm Petri dishes and cultured for 24 h in MEM containing 2 % FCS. Cells were then detached by incubation with PBS containing 5 mM EDTA at 37°C for 5 min and centrifuged at 300 g for 5min. The dry pellet was stored at -80°C until analysis. Mass spectrometry analysis was performed on a hybrid quadrupole-TOF mass spectrometer Triple TOF 5600+ (Sciex, Redwood City, CA, USA). For trypsin digestion, cell pellets were resuspended in 200 µL of Rapigest SF (Waters, Milford, MA, USA). Then, 5 mM (final concentration) dithiothreitol (DTT) (AppliChem, Darmstadt, Germany) was added to each reaction tube. The samples were then incubated at 95°C for 10 min and cooled to room temperature. Cysteine residues were alkylated by adding 200 mM of MMTS (10 mM final concentration) with a further ten-minute incubation at 37°C. Trypsin (Sigma, Saint-Quentin-Fallavier, France) was added to the sample at a 1:25 w/w ratio (enzyme/protein), and the mixture was incubated at 37°C overnight. The reaction was quenched by adding 23 µL of formic acid (9 % final concentration) and incubated at 37°C for one hour. The acid-treated samples were centrifuged at 16,000 g for 10 min. The supernatant was transferred into new reaction tubes and peptide solutions were desalted using self-packed C18 STAGE tips. Micro BCA assay was performed and peptides were vacuum-dried in a SpeedVac concentrator and stored at -20°C until measured by LC-MS/MS. Immediately prior to micro-LC, the fractions were resuspended in H2O with 0.1 % v/v formic acid at a concentration of 1 µg/µL.

Each sample (5 µg) was separated into a micro 2D-LC 425 system (Eksigent) using a ChromXP C18CL column (3 µm, 120 A, 15×0.3 cm, Sciex) at a flow rate of 5 µL/min. Water and acetonitrile both containing 0.1 % formic acid, were used as solvents A and B, respectively. The following gradient of solvent B was used: 0 to 5 min~~utes~~ 5 % B, 5 to 75 minutes 5 % to 35 % B, then 10 min at 95 % B, and finally 10 min at 5 % B for column equilibration. As the peptides eluted, they were directly injected into the Triple TOF 5600 + operated with a 'top 30' data-dependent acquisition (DDA) system using positive ion mode. The acquisition mode consisted of a 250-ms survey MS scan from 400 to 1250 *m/z*, followed by an MS/MS scan from 230 to 1500 *m/z* (75 ms acquisition time, 350 mDa mass tolerance, rolling collision energy) of the top 30 precursor ions from the survey scan.

For the relative quantification by SWATH-MS acquisition, each sample (5 µg) was analyzed using the LC-MS equipment and LC gradient described above for building the spectral library, but using a SWATH-MS acquisition method. The method consisted of repeating the whole gradient cycle, involving the acquisition of 32 TOF MS/MS scans of overlapping sequential precursor isolation windows (25 *m/z* isolation width, 1 m/z overlap, high-sensitivity mode) covering the 400 to 1200 m/z mass range, with a previous MS scan for each cycle. The accumulation time was 50 ms for the MS scan (from 400 to 1200 *m/z*) and 100 ms for the product ion scan (230 to 1500 *m/z*), giving a 3.5 s total cycle time. Peak extraction of the SWATH data was performed using SpectronautTM Pulsar X 13 software with default analysis settings. Retention time prediction type was set to dynamic iRT and calibration mode was set to automatic. These settings also included mutated decoy method and cross run normalization enabled. The FDR (false discovery rate) was estimated with the mProphet approach and Q-value cut-off for both precursor and protein was set to 1 %. Interference correction was enabled for quantification which required a minimum of 2 precursor-ions and 3 fragment-ions. The term protein refers to protein groups as determined by the algorithm implemented in SpectronautTM.

Statistical analysis

Data are presented as the mean values ± standard deviation, from at least 3 independent experiments with at least 3 replicates per experiment, unless otherwise stated. Statistical significance was measured with GraphPad Prism software (GraphPad software ver 8.0.1.244, Inc.,

La Jolla, CA, USA) using the unpaired two-tailed student's *t*-test, or ANOVA test with a *p* value of 0.05 or less considered as statically significant. For proteomic analysis, Q-value less than 0.05 was considered as significant.

Results

Chemotherapy persistent TNBC cells displayed enhanced cell growth both in vitro and in vivo

We first established persistent TNBC cell models after treating MDA-MB-231 and SUM159-PT TNBC cell lines with epirubicin plus cyclophosphamide, and then with paclitaxel for a total of 18 weeks (Fig. 1A). No morphological change was observed compared to parental cells (not shown). When cells were cultured in monolayer for 4 days, both MDA-MB-231 and SUM159-PT persistent cells exhibited an increased cell growth (Fig. 1B). Clonogenic assay with cells cultured at low density showed a more proliferative phenotype of persistent cells (Fig. 1C). The increased proliferative ability of persistent cells was also observed when cells were cultured in 3D Matrigel® (Fig. 1D). Finally, when MDA-MB-231 control and persistent cells were subcutaneously injected in SCID mice, a faster growth was observed for tumors formed by persistent cells (Fig. 1E).

MDA-MB-231 persistent cells were less sensitive to chemotherapeutic drugs

In order to investigate if persistent cells were still sensitive to chemotherapeutic drugs, both MDA-MB-231 and SUM159-PT were submitted to either combined and sequential treatment with epirubicin, cyclophosphamide and paclitaxel, or to treatment with epirubicin or paclitaxel alone (Fig. 2). As shown in Fig. 2A, when MDA-MB-231 cells were treated with epirubicin and cyclophosphamide for 48 h, and then with paclitaxel for another 48 h, control cells exhibited about 50 % of growth inhibition as expected, while growth of persistent cells was no longer inhibited by such a treatment. When cells were treated with epirubicin or paclitaxel alone for 96 h, MDA-MB-231 persistent cells were less sensitive to the drugs compared to control cells (Fig. 2B and C), with IC-50 values being about 2 to 3 fold higher than that of control (Fig. 2C). In contrast, no difference in cell growth inhibition was observed between SUM159-PT control and persistent cells whatever drug treatment (Fig. 2A-C), indicating that SUM159-PT persistent cells maintained the same sensitivity to the drugs.

MDA-MB-231 persistent cells exhibited an enhanced OXPHOS profile

Increasing data point out the importance of metabolism adapatation in TNBC progression and resistance to therapies. We determined if TNBC persistent cells surviving chemotherapy displayed any modifications in terms of bioenergetic profile. Mitchondrial function was determined indirectly through oxygen consumption rate (OCR) which reflects the mitochondrial respiration (OXPHOS) (Fig. 3). MDA-MB-231 persistent cells exhibited eleved OCR in both basal and stressed conditions (maximal OCR) compared to control cells; increases in proton leak, in OCR related to ATP production and in spare respiratory capacity were also observed in persistent cells (Fig. 3A, Fig.S1A-B). Higer maximal OCR was also observerd in tumor-derived MDA-MB-231 persistent cells compared to tumor-derived naive MDA-MB-231 cells (Fig. 3C), indicating the stable modification of mitochondrial plasticity. However, neither the mitochondrial mass (Fig. S2A), nor the levels of respiratory chain complex proteins were modified in MDA-MB-231 persistent cells compared to control cells (Fig. S2B), suggesting that OXPHOS increase in MDA-MB-231 persisters was independent of mitochondrial biogenesis. We next evaluated the glycolytic activity, which was measured indirectly by the extracellular acidification rate (ECAR). No difference was observed between MDA-MB-231 control and persistent cells (Fig. 3D), suggesting that OXPHOS operates at a higher rate without requiring a proportional increase in glycolysis. The bioenergetic map comparing the levels of OCR and ECAR further showed that MDA-MB-231 persistent cells used OXPHOS in response to a highly energetic demand (Fig. 3D). Contrary to MDA-MB-231 cells, SUM159-PT control and persistent cells showed similar levels of basal and maximal OCR (about 400 $pmol.min^{-1}.10^5$ $cells^{-1}$) (Fig. 3B, Fig. S1C-D). The bioenergetic map comparing the levels of OCR and ECAR further showed that SUM159-PT cell line was not metabolically flexible (Fig. S1E).

MDA-MB-231 persistent cells required mitochondrial pyruvate metabolism to maintain higher OXPHOS

As MDA-MB-231 persistent cells exhibited reduced sensitivity to chemotherapeutic drugs and enhanced OXPHOS, we next performed proteomics and metabolomics to clarify the underlying molecular mechanisms of adapdation in persistent cells. Proteomic analysis showed significant modifications of 1081 proteins in persistent cells when compared to control cells (Table sup1). Significant modifications of proteins known to be involved in macromolecular metabolisms and mitochondrial fonctions are listed in Fig 4A. Several proteins were found to be increased at least 100 % compared to control cells. These included OXCT1 (Succinyl-CoA:3-ketoacid coenzyme A transferase 1) (2.78 fold-change; Q-value: 0.0008), PMPCA (Mitochondrial processing peptidase subunit alpha) (3.26 fold-change; Q- value: 4.01E-06), COX17 (Cytochrome c oxidase copper chaperone) (2.03 fold-change; Q-value: 0.0003), and IDH3G (Isocitrate dehydrogenase [NAD] subunit gamma) (2.27 fold-change; Q-value: 1.43E-07). Meawhile, other proteins were found to be significantly downregulated. These included CAVIN3 (Caveolae-associated protein 3) (0.44 fold-change; Q-value: 7.04E-05), NNT (NAD(P) transhydrogenase) (0.62 fold-change; Q-value: 5.63E-12), NDUFAF2 (NADH dehydrogenase ubiquinone 1 alpha)(0.43 fold-change; Q-value: 0.02), and SDHA (Succinate dehydrogenase ubiquinone flavoprotein subunit alpha) (0.61 fold-change; Q- value: 2.92E-14).

Metabolomic analysis showed increased levels of metabolites from both glycolysis and TCA cycle in MDA-MB-231 persistent cells (Fig. 4B). Of note, a significant pyruvate increase in persistent cells was not associated with a significant change in lactic acid production, suggesting that pyruvate was preferentially used in TCA cycle rather than aerobic glycolysis. Combined analysis of data from proteomics and metabolomics, using Metaboanalyst site and Joint Pathway module identified TCA cycle among the most activated pathways in MDA-MB-231 persistent cells (Fig. 4C).

To further investigate the importance of pyruvate metabolism in OXPHOS of MDA-MB-231 persistent cells, we determined OCR in full OXPHOS medium (containing glutamine, glucose and pyruvate) and in OXPHOS medium containing only glutamine (Fig. 4D). The absence of glucose and pyruvate significantly reduced both basal and maximal OCR in MDA-MB-231 persistent cells, indicating the requirement of glucose and pyruvate to maintain elevated OXPHOS in persistent cells. We then treated cells for 30 min before OCR measurement with BPTES or/and UK-5099, the inhibitors of glutaminase and mitochondrial pyruvate carriers (MPC), respectively. Inhibition of glutaminase did not modify either basal OCR or maximal OCR in control cells, but significantly reduced maximal OCR in persistent cells, suggesting that persistent cells may need glutamine to maintain OXPHOS in stressed condition. On the other hand, the inhibition of pyruvate entry into the mitochondria by UK-5099 dit not affect basal OCR in control cells, but significantly reduced maximal OCR, suggesting that mitochondrial pyruvate metabolism was necessary to maintain OXPHOS in control cells under stressed condition. Interestingly, inhibition of pyruvate entry into mitochondria reduced both basal and maximal OCR in MDA-MB-231 persistent cells, indicating the increased requirement of mitochondrial pyruvate metabolism in persisters. Moreover, incubation of cells with UK-5099 and BPTES together did not further reduce OCR when compared to cells treated with each inhibitor alone (Fig. 4). Taken together, these data suggested that glutamine and especially pyruvate

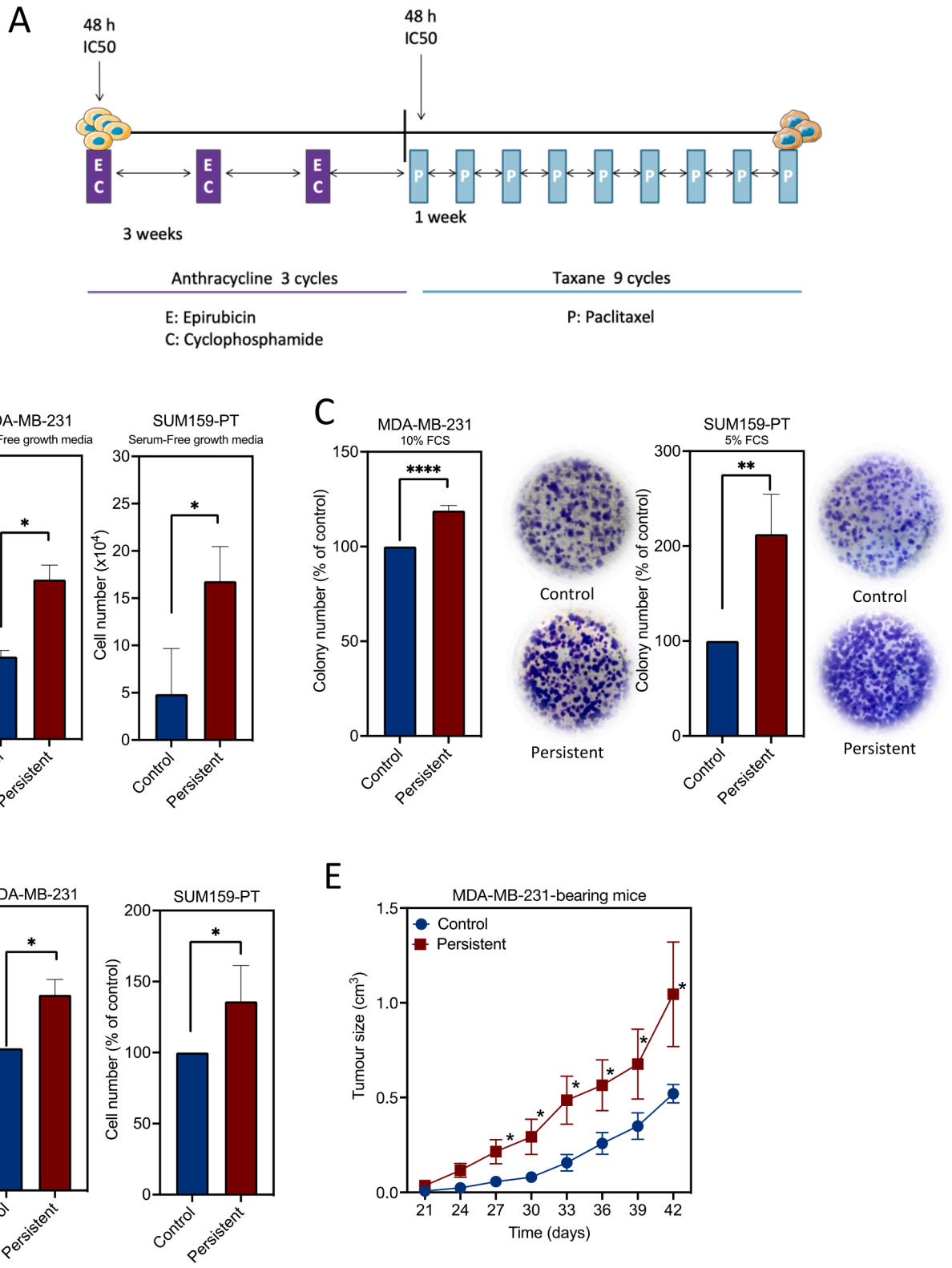

1. Establishment and phenotype characterization of persistent cells *in vitro and in vivo*. (**A**) Protocol for the establissement of MDA-MB-231 and SUM159-PT persistent cells. (**B**) Control and persistent cells were cultured in serum-free culture media for 96 h. The number of viable cells was determined using a hemocytometer after incubation with trypan blue. (**C**) Colony formation. Control and persistent cells were cultured in culture media containing 2 % FCS for 10 days. Colony number was counted after crystal violet staining. (**D**) Cell growth in 3D Matrigel. Cells were seeded in a mix solution of media containing 1 % FCS and Matrigel (v:v, 1:1) to form a droplet, and then cultured in media containing 10 % FCS for 10 days. At the end of the culture, cells were extracted from Matrigel and counted with a hemocytometer. Scale bar 250 μm. Quantitative graphics (**B-D**) correspond to at least 3 independent experiments and the illustrations are representative of 3 independent experiments. *, $p < 0.05$; **, $p < 0.01$; ***, $p < 0.001$. Unpaired Student t-test. (**E**) Tumor growth in SCID mice xenograft model. MDA-MB-231 control and persistent cells were subcutaneously injected in SCID mice (n=5 for each condition) as described in materials and methods. Tumor volume was measured every 3 days. The error bars present standard error mean (SEM). *, $p<0.05$, Unpaired Student *t*-test.

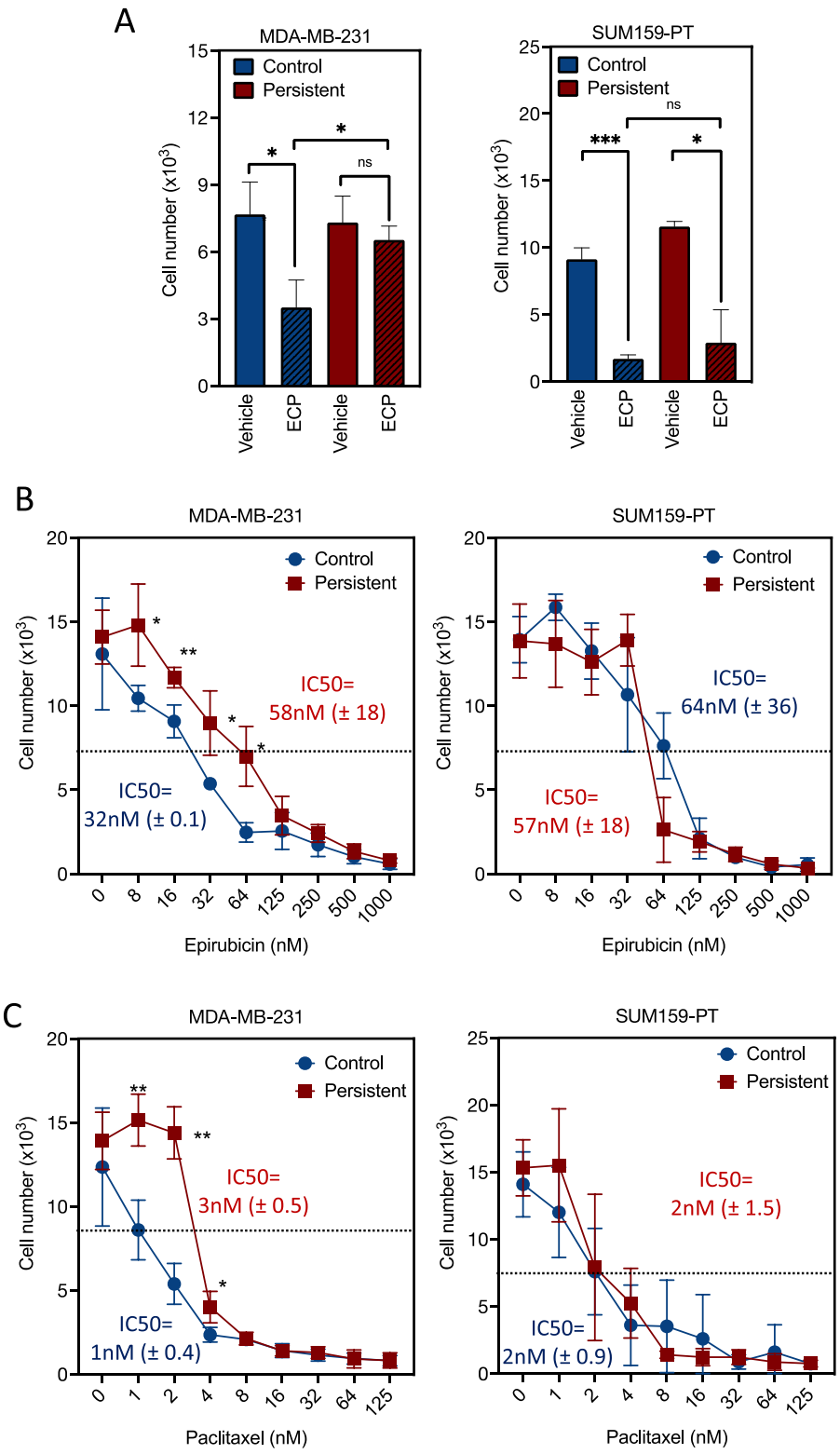

2. Sensibilities of persistent cells to chemotherapeutic drugs. (**A**) MDA-MB-231 and SUM159-PT control and persistent cells were first treated with epirubicin (E) and cyclophosphamide (C) for 48 h, and then with paclitaxel (P) for another 48 h as described in materials and methods for the establishment of persistent cell models. At the end of the treatment, cells were then stained with Hoestch 33342 and counted using Celigo. (**B** and **C**) Cells were treated with different concentrations of epirubicin (**B**) or paclitaxel (**C**) for 96 h, cells were then stained with Hoestch 33342 and counted using Celigo. The graphics and the curves are representatives of at least 3 independent experiments. *, $p<0.05$; **, $p<0.01$; ***, $p<0.001$. ANOVA test.

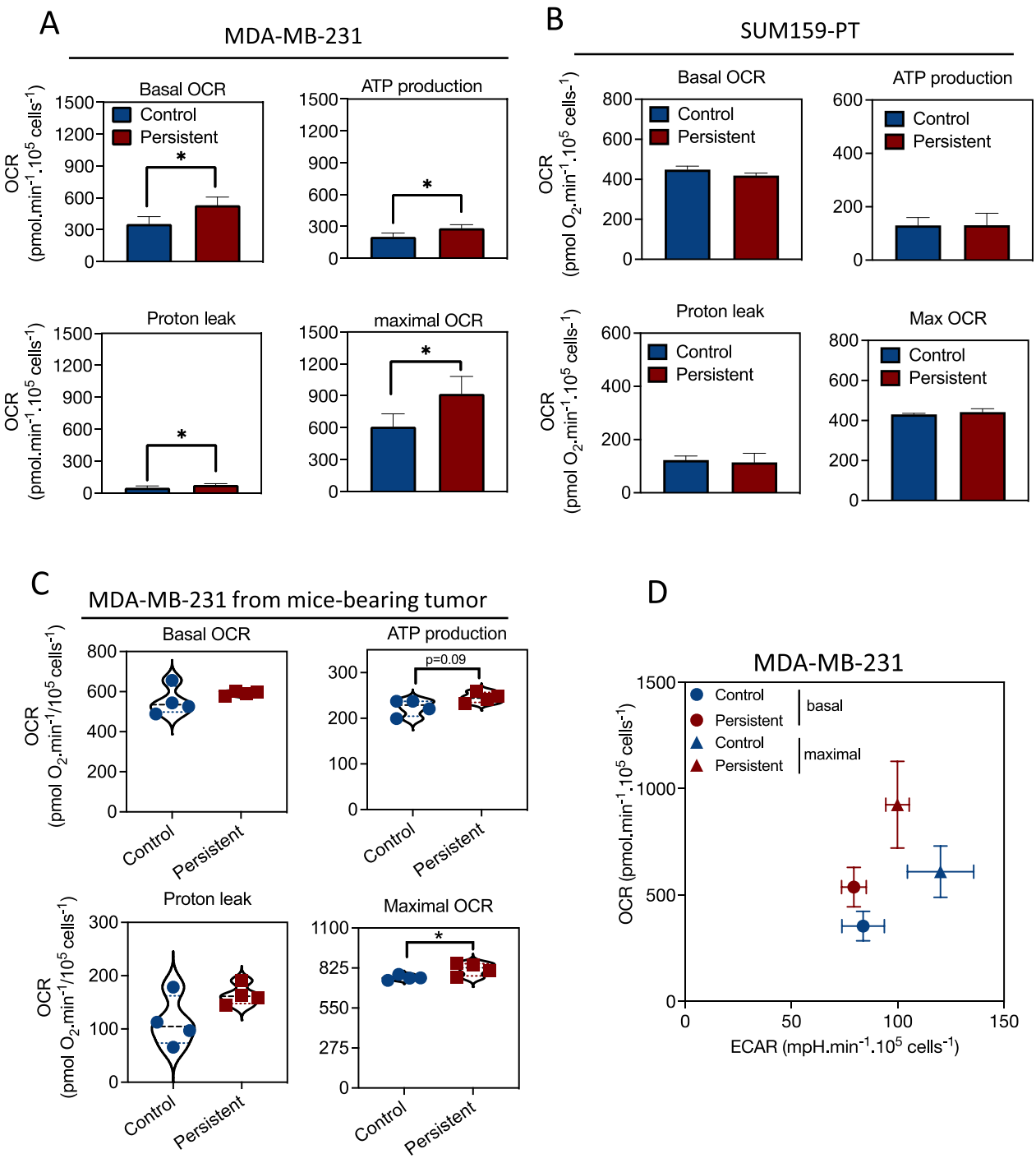

3. Metabolic properties of persistent cells. (**A**) OXPHOS parameters of MDA-MB-231 control and persistent cells. Oxygen Consumption Rate (OCR) measurements were obtained using an extracellular flux analyzer (Seahorse Bioscience). Bioenergetics parameters of cancer cells have been obtained by adding the ATP synthase inhibitor Oligomycin A (1 μM) to derive ATP-linked OCR, FCCP to uncouple the mitochondria for maximal OCR, and antimycin A and rotenone to assess non mitochondrial respiration. (**B**) OXPHOS parameters of SUM159-PT control and persistent cells. (**C**) OXPHOS parameters of MDA-MB-231 cells derived from xenografted tumors. MDA-MB-231 control and persistent cells were subcutaneously xenografted in SCID mice. At the end of the experiments, tumors were dissociated and the resulting tumor cells were cultured as described in materials and methods before the measurement of OXPHOS parameters.→ (**D**) Bioenergetics profiles of the MDA-MB231 cells by plotting Basal and Maximal ECAR and OCR levels. The quantitative graphics and the curves are representatives of at least 3 independent experiments. *, $p<0.05$. Unpaired student *t*-test.

were needed to maintain the higher OXPHOX profile in MDA-MB-231 persistent cells.

Enhanced growth inhibition by concomitant application of UK-5099 and chemotherapeutic drugs in MDA-MB-231 persistent cells

In order to determine if OXPHOX targeting can increase the sensitivity of persistent cancer cells to chemotherapeutic drugs, we first determined the number of viable cells. As shown in Fig. 5A, when

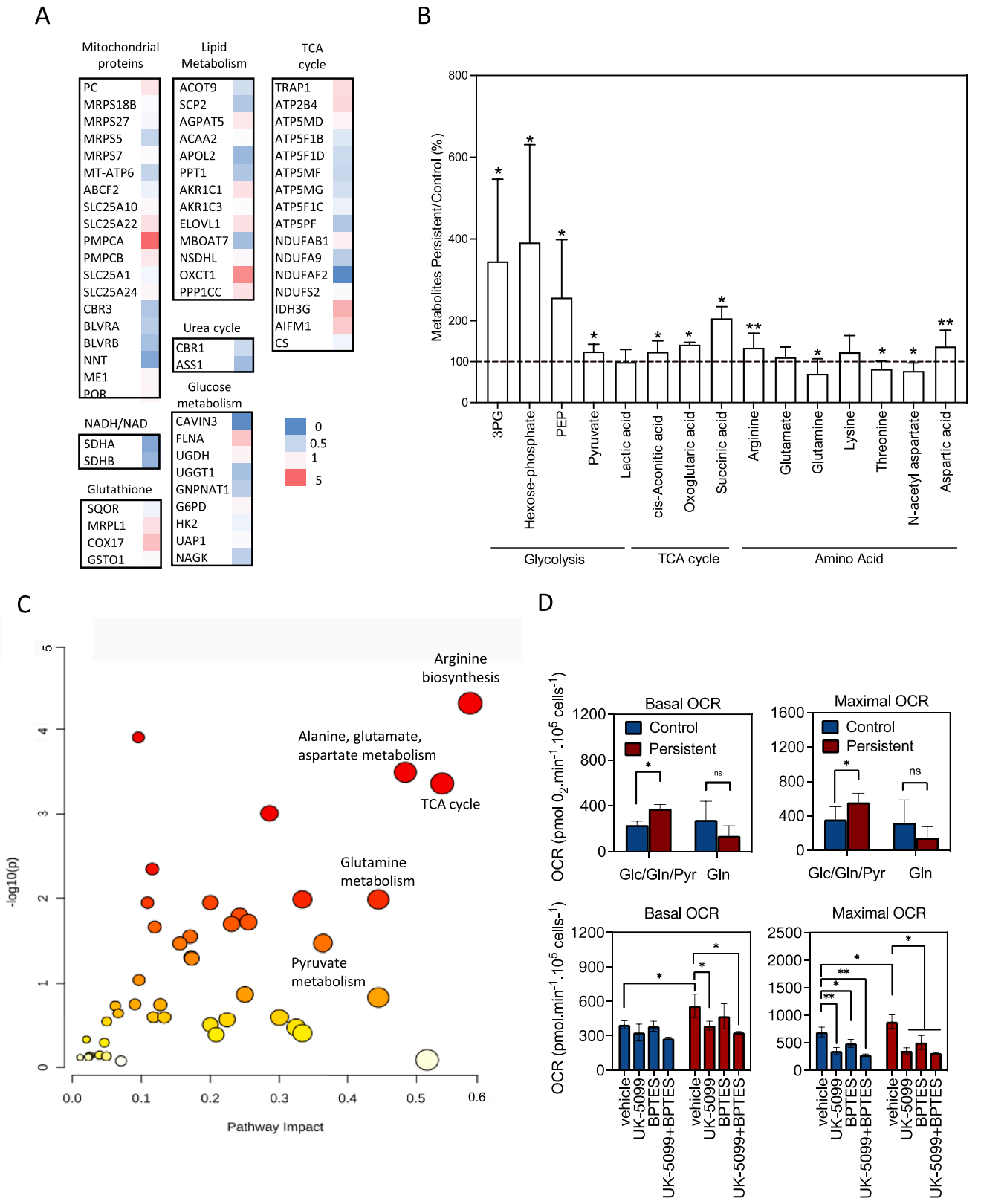

4. Pyruvate metabolism supports enhanced mitochondrial respiration in persistent MDA-MB-231 cells (**A**) Heatmap showing the ratio of significantly modified proteins (persistent to control) involved in respiratory chain. Proteins extracted from control and persistent cells were analyzed by tandem mass spectrometry (MS/MS). (**B**) Metabolomic intermediates analyzed by mass spectrometry. (**C**) proteomics and metabolomics integration showing the enrichment (-log10 (P)) and the importance (Pathway impact) of dysregulated signaling pathways in MDA-MB-231 persistent cells. The graph was produced using the Metaboanalyst site and the Joint Pathway module. (**D**) OCR measurement in MDA-MB-231 cells under different conditions: OXPHOS medium containing glucose (Glu), glutamine (Gln) and pyruvate (Pyr) *vs* the medium containing only glutamine; in the presence or absence of 3 μM BPTES (inhibitor of glutaminase) and/or 10 μM UK-5099 (inhibitor of mitochondrial pyruvate carriers). Quantitative graphics and the curve were representatives at least 3 independent experiments. *, $p<0.05$; **, $p<0.01$. Unpaired student *t*-test.

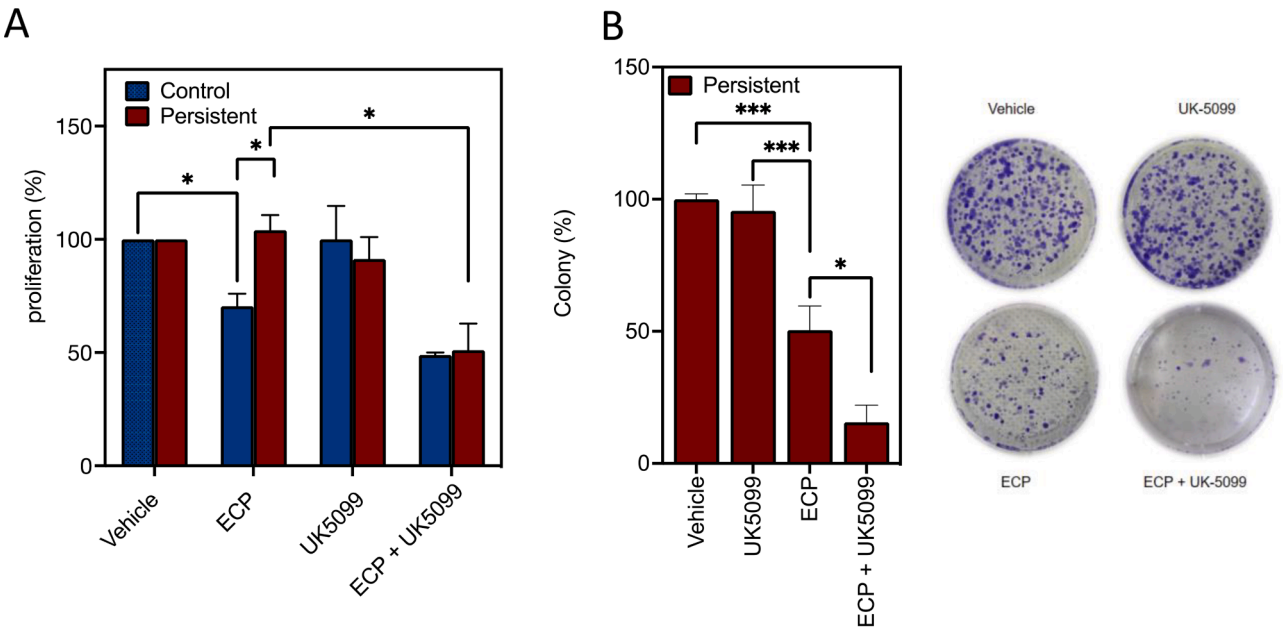

C

OXPHOS inhibitor	Chemotherapy drug	Cell line	Bliss synergy score (*p*value)	Effect
UK-5099	Epirubicin	MDA-MB-231 Control	21.9 (1.87e-04)	Synergistic
		MDA-MB-231 Persistent	22.2 (4,56e-03)	Synergistic

5. Impact of OXPHOS reduction on chemotherapy-induced growth inhibition of MDA-MB-231 persistent cells. (**A**) Persistent cells were cultured in the presence or absence of 10 μM UK-5099 for 96 h. Cells were then stained with Hoestch 33342 and counted using Celigo. (**B**). Colony formation of persistent cells cultured in the presence or absence of 10 μM UK-5099 for 10 days. (**C**). Bliss synergy score for inhition of cell frowth combining tigecycline or UK-5099 with epirubicin. The Bliss synergy score was determined under viability percentage with "synergyfinder" of R software. Threshold : Synergistic =]20; infinity[; Additive = [20; -20[; Antagonist = [-20; infinity].
Quantitative graphics are representatives at least 3 independent experiments and the illustrations (B) are representative of 3 independent experiments. *, $p<0.05$, ***, $p<0.001$. ANOVA test.

persistent cells were concomitantly treated with UK-5099 and chemotherapeutic drugs (ECP treatment: epirubicin and cyclophosphamide for 48 h, and paclitaxel for another 48 h), a significant inhibition of persistent cell growth was observed whereras neither UK-5099, nor ECP affected cell growth. Similar results were also obtained with colony formation assay (Fig. 5B). When persistent cells were concomitantly treated with BPTES and ECP, no significant reduction of colony formation was observed compared to ECP treatment alone (Fig. S3). Co-treatment with the two inhibitors and ECP did not further reduce colony formation compared to co-treatment with UK-5099 alone and ECP (Fig. S3). Finally, when persistent cells were co-treated with UK-5099 and different concentrations of epirubicine, a synergistic inhibition of cell growth was observed (Fig. 5C). All these data indicated that reducing OXPHOS in persistent cells without affecting cell viability was sufficient to re-sensitize these cells to chemotheraputic drugs.

Discussion

The high rate of recurrence and mortality after neoadjuvant chemotherapy in TNBC emphasizes the need to identify vulnerabilities of cancer cells surviving chemotherapy. This study aimed to generate a relevant chemotherapy persistent cellular model mimicking clinical neoadjuvant treatment, and to unveil molecular and metabolic modifications of TNBC cells surviving combinatory and sequential chemotherapeutic treatment. We found that persistent cells of both mesenchymal MDA-MB-231 cells and claudin-low SUM159-PT cells displayed enhanced cell growth both *in vitro* and *in vivo* in xenograft SCID mouse model suggesting the acquisition of a more aggressive phenotype of chem-persistent cells.

Interestingly, MDA-MB-231 persistent cells became less sensitive to chemotherapeutic drugs, whereas the SUM159-PT persistent cells kept similar drug sensitivity compared to their naive counterparts. Our findings are supported by clinical observations reporting that not all recurrent TNBC patients become resistant to chemotherapy, since *de novo* treatment with the same drugs can again produce a pCR [21]. The unaltered drug sensitivity in SUM159-PT persistent cells is also in line with the recent concept of drug tolerance, which indicates that residual cancer cells surviving chemotherapy do not present the phenotype of drug resistance. Drug tolerance may be induced by therapeutic agents through non-genetic reprogramming that leads to a reversible state [7, 22-23]. On the other hand, energetic metabolism reprogramming has been increasingly reported to be involved in both drug resistance and drug tolerance [24–25]. Herein, we found that MDA-MB-231 persistent cells displayed an enhanced OXPHOS profile, whereas SUM159-PT persistent cells exhibited a similar OXPHOS function, compared to their naive counterparts. Moreover, no difference was observed between

basal and maximal OCR levels, in both control and persistent SUM159-PT cells, suggesting that these cells which already present relative high levels of basal OCR were no longer able to further increase OXPHOS under stressed conditions. Our findings are consistent with previous work by Lee and colleagues [10] and highlight different OXPHOS profiles according to molecular subtypes of TNBC cells.

The association between the enhanced OXPHOS and the reduced drug sensitivity in MDA-MB-231 persistent cells prompted us to further analyze protein and metabolic modifications in these cells. We found that MDA-MB-231 persistent cells displayed an enhancement of TCA cycle activity and pyruvate production, without any change in mitochondrial mass. We also observed an increase of spare respiratory capacity in persistent cells. This increase may result from improved mitochondrial function, such as optimizing the efficiency of the electron transport chain (ETC), which enables mitochondria to use oxygen more efficiently to generate ATP [26].

In addition, MDA-MB-231 persistent cells required mitochondrial pyruvate metabolism to maintain higher levels of OXPHOS. Treatment of persistent cells with UK-5099, an inhibitor of mitochondrial pyruvate carriers, at a concentration that decreased OXPHOS level without affecting cell survival was sufficient to re-sensitize these cells to chemotherapeutic drugs. Our data suggested that the enhanced mitochondrial pyruvate metabolism contributed to the reduced drug sensitivity of persistent TNBC cells. In line with our findings, Echeverria and colleagues, by analyzing tumor samples in patient-derived xenograft (PDX) models and biopsies from TNBC women, have reported that residual tumors following neoadjuvant treatment with doxorubicin and cyclophosphamide exhibit high OXPHOS profile compared to treatment-naive tumors [7]. OXPHOS inhibition by IACS-010759, which targets the complex I of the mitochondria respiratory chain, delays tumor growth and the regrowth of chemotherapy-treated residual tumors in the PDX models. In addition, a synerigistic inhibition on tumor growth is obtained when IACS-010759 is applied after treatment with chemotherapy drugs, suggesting that a sequential regimen consisting of chemocherapy followed by IACS-010759 could prolong duration of response to chemotherapy in TNBC. Not only chemotherapy persistent cells present such a metabolic vulnerability, chemotherapy resistant cancer cells can be also targeted through OXPHOS inhibition. For example, the association of IACS-010759 with Palbociclib, an inhibitor of CDK4/6, or carbozantinib, a kinase inhibitor, showed synergistic effect on cell growth in chemotherapy resistant TNBC cells [27]. Thus, targeting mitochondrial metabolism dependency holds great promise to improve the outcome of chemotherapy in TNBC. However, the diversity of TNBC subtypes renders such therapeutic strategies challenging. Using a multi-omics database of 465 patient biopsies, Gong and colleagues have revealed the metabolic heterogeneity of TNBCs [28]. The lipogenic TNBC subtype with upregulated lipid metabolism is more sensitive to metabolic inhibitors targeting fatty acid synthesis, whereas the glycolytic TNBC subtype with upregulated carbohydrate and nucleotide metabolism shows higher sensitivity to inhibitors targeting glycolysis. Interestingly, inhibition of lactate dehydrogenase can enhance the tumor response to anti-PD-1 immunotherapy in the glycolytic subtype of TNBC [28]. Furthermore, the same metabolite can be used differently, depending on intrinsic cancer cell type and the influence of the microenvironment. This is the case for pyruvate, which can be used by cancer cells either *via* glycolysis or *via* oxidative phosphorylation (OXPHOS). On the one hand, pyruvate can form lactate, through lactate dehydrogenase A, to ensure total aerobic glycolysis; on the other hand, pyruvate can be transferred into mitochondria by mitochondrial pyruvate carriers and then converted to acetyl-coenzyme A, by the pyruvate dehydrogenase, before incorporation into the TCA cycle.

Apart from diverse intrinsic metabolic adaptabilities of TNBC cells, chemotherapy can also illicit different modifications of metabolism. For example, resistance to doxorubicin is linked to glutathione metabolism, whereas resistance to epirubicin is tied to enhanced mitochondrial bioenergetic capacity [29]. More recently, Beak and colleagues have described that DNA-damaging agents increased mitochondrial elongation, mitochondrial content, flux of glucose through the TCA cycle, and OXPHOS, whereas taxanes instead decreased mitochondrial elongation and OXPHOS [30]. In our work, we found that the increased flux of TCA cycle and OXPHOS in persistent MDA-MB-231 cells were not accompanied by mitochondrial mass modification. It is clear that further investigations of functional metabolic adaptations are needed to better stratify TNBC subtypes in order to improve the efficiency of chemotherapy by targeting specific metabolic vulnerabilities.

Conclusions

In this work, we established a model of persistent triple negative breast cancer cells after combined and sequential treatment with therapeutic drugs. We observed that the chemo-persistent cells were more proliferative, with MDA-MB-231 persistent cells becoming less sensitive to chemotherapeutic drugs compared to the parental ones. These persistent cells presented a more pyruvate dependent profile that maintained an increased mitochondrial spare respiratory capacity. Our findings give some insights on the mechanisms developed by persistent cancer cells in response to chemotherapy, and suggest that targeting mitochondrial pyruvate metabolism may help to overcome mitochondrial adaptation in triple negative breast cancer cells.

CRediT authorship contribution statement

Marie Winter: Methodology, Investigation, Data curation, Validation, Visualization, Writing – original draft, Writing – review & editing. **Amina Nait Eldjoudi:** Methodology, Investigation, Data curation, Validation, Visualization, Writing – original draft, Writing – review & editing. **Catherine Guette:** Investigation, Data curation, Validation, Visualization, Writing – original draft, Writing – review & editing. **Hubert Hondermarck:** Conceptualization, Validation, Writing – review & editing. **Roland P. Bourette:** Investigation, Validation, Writing – review & editing. **Quentin Fovez:** Investigation, Validation. **William Laine:** Investigation, Validation. **Bart Ghesquiere:** Data curation, Validation. **Eric Adriaenssens:** Funding acquisition, Investigation, Validation, Writing – review & editing. **Jérôme Kluza:** Conceptualization, Funding acquisition, Resources, Supervision, Writing – original draft, Writing – review & editing. **Xuefen Le Bourhis:** Conceptualization, Funding acquisition, Resources, Supervision, Writing – original draft, Writing – review & editing.

Declaration of Competing Interest

The authors declare that they have no known competing financial interests or personal relationships that could have appeared to influence the work reported in this paper.

Funding

This work was supported by funding from the Ligue contre le Cancer Septentrion committee and a grant form Contrat de Plan Etat-Région CPER Cancer 2015–2020.

Supplementary materials

Supplementary material associated with this article can be found, in the online version, at doi:10.1016/j.neo.2023.100949.

References

[1] NM. Almansour, Triple-negative breast cancer: a brief review about epidemiology, risk factors, signaling pathways, treatment and role of artificial intelligence, Front. Mol. Biosci. 9 (2022), 836417, https://doi.org/10.3389/fmolb.2022.836417.

[2] X Bai, J Ni, J Beretov, P Graham, Y. Li, Triple-negative breast cancer therapeutic resistance: where is the Achilles' heel? Cancer Lett. 497 (2021) 100–111, https://doi.org/10.1016/j.canlet.2020.10.016.

[3] C Liedtke, C Mazouni, KR Hess, F André, A Tordai, JA Mejia, WF Symmans, AM Gonzalez-Angulo, B Hennessy, M Green, M Cristofanilli, GN Hortobagyi, L. Pusztai, Response to neoadjuvant therapy and long-term survival in patients with triple-negative breast cancer, J. Clin. Oncol. 26 (8) (2008) 1275–1281, https://doi.org/10.1200/JCO.2007.14.4147.

[4] G von Minckwitz, M Untch, JU Blohmer, SD Costa, H Eidtmann, PA Fasching, B Gerber, W Eiermann, J Hilfrich, J Huober, C Jackisch, M Kaufmann, GE Konecny, C Denkert, V Nekljudova, K Mehta, S. Loibl, Definition and impact of pathologic complete response on prognosis after neoadjuvant chemotherapy in various intrinsic breast cancer subtypes, J. Clin. Oncol. 30 (15) (2012) 1796–1804, https://doi.org/10.1200/JCO.2011.38.8595.

[5] P Cortazar, L Zhang, M Untch, K Mehta, JP Costantino, N Wolmark, H Bonnefoi, D Cameron, L Gianni, P Valagussa, SM Swain, T Prowell, S Loibl, DL Wickerham, J Bogaerts, J Baselga, C Perou, G Blumenthal, J Blohmer, EP Mamounas, J Bergh, V Semiglazov, R Justice, H Eidtmann, S Paik, M Piccart, R Sridhara, PA Fasching, L Slaets, S Tang, B Gerber, CE Geyer Jr, R Pazdur, N Ditsch, P Rastogi, W Eiermann, G. von Minckwitz, Pathological complete response and long-term clinical benefit in breast cancer: the CTNeoBC pooled analysis, Lancet 384 (9938) (2014) 164–172, https://doi.org/10.1016/S0140-6736(13)62422-8.

[6] WF Symmans, C Wei, R Gould, X Yu, Y Zhang, M Liu, A Walls, A Bousamra, M Ramineni, B Sinn, K Hunt, TA Buchholz, V Valero, AU Buzdar, W Yang, AM Brewster, S Moulder, L Pusztai, C Hatzis, GN Hortobagyi, Long-term prognostic risk after neoadjuvant chemotherapy associated with residual cancer burden and breast cancer subtype, J. Clin. Oncol. 35 (10) (2017) 1049–1060, https://doi.org/10.1200/JCO.2015.63.1010.

[7] GV Echeverria, Z Ge, S Seth, X Zhang, S Jeter-Jones, X Zhou, S Cai, Y Tu, A McCoy, M Peoples, Y Sun, H Qiu, Q Chang, C Bristow, A Carugo, J Shao, X Ma, A Harris, P Mundi, R Lau, V Ramamoorthy, Y Wu, MJ Alvarez, A Califano, SL Moulder, WF Symmans, JR Marszalek, TP Heffernan, JT Chang, Piwnica-Worms H. Resistance to neoadjuvant chemotherapy in triple-negative breast cancer mediated by a reversible drug-tolerant state, Sci. Transl. Med. 11 (488) (2019) eaav0936, https://doi.org/10.1126/scitranslmed.aav0936.

[8] L Yin, JJ Duan, XW Bian, SC. Yu, Triple-negative breast cancer molecular subtyping and treatment progress, Breast Cancer Res. 22 (1) (2020) 61, https://doi.org/10.1186/s13058-020-01296-5.

[9] P Schmid, S Adams, HS Rugo, A Schneeweiss, CH Barrios, H Iwata, V Diéras, R Hegg, SA Im, G Shaw Wright, V Henschel, L Molinero, SY Chui, R Funke, A Husain, EP Winer, S Loi, LA Emens, IMpassion130 Trial Investigators, Atezolizumab and Nab-Paclitaxel in advanced triple-negative breast cancer, N. Engl. J. Med. 379 (22) (2018) 2108–2121, https://doi.org/10.1056/NEJMoa1809615.

[10] KM Lee, JM Giltnane, JM Balko, LJ Schwarz, AL Guerrero-Zotano, KE Hutchinson, MJ Nixon, MV Estrada, V Sánchez, ME Sanders, T Lee, H Gómez, A Lluch, JA Pérez-Fidalgo, MM Wolf, G Andrejeva, JC Rathmell, SW Fesik, CL. Arteaga, MYC and MCL1 cooperatively promote chemotherapy-resistant breast cancer stem cells via regulation of mitochondrial oxidative phosphorylation, Cell Metab. 26 (4) (2017) 633–647, https://doi.org/10.1016/j.cmet.2017.09.009.

[11] S Liu, Y Li, M Yuan, Q Song, M. Liu, Correlation between the Warburg effect and progression of triple-negative breast cancer, Front. Oncol. 12 (2023), 1060495, https://doi.org/10.3389/fonc.2022.1060495.

[12] Q Li, T Qin, Z Bi, H Hong, L Ding, J Chen, W Wu, X Lin, W Fu, F Zheng, Y Yao, ML Luo, PE Saw, GM Wulf, X Xu, E Song, H Yao, H. Hu, Rac1 activates non-oxidative pentose phosphate pathway to induce chemoresistance of breast cancer, Nat. Commun. 11 (1) (2020) 1456, https://doi.org/10.1038/s41467-020-15308-7.

[13] M Luo, A Fu, R Wu, N Wei, K Song, S Lim, KQ. Luo, High expression of G6PD increases doxorubicin resistance in triple negative breast cancer cells by maintaining GSH level, Int. J. Biol. Sci. 18 (3) (2022) 1120–1133, https://doi.org/10.7150/ijbs.65555.

[14] BA Webb, M Chimenti, MP Jacobson, DL. Barber, Dysregulated pH: a perfect storm for cancer progression, Nat. Rev. Cancer 11 (9) (2011) 671–677, https://doi.org/10.1038/nrc3110.

[15] B Győrffy, V Serra, K Jürchott, R Abdul-Ghani, M Garber, U Stein, I Petersen, H Lage, M Dietel, R. Schäfer, Prediction of doxorubicin sensitivity in breast tumors based on gene expression profiles of drug-resistant cell lines correlates with patient survival, Oncogene 24 (51) (2005) 7542–7551, https://doi.org/10.1038/sj.onc.1208908.

[16] J Kenicer, M Spears, N Lyttle, KJ Taylor, L Liao, CA Cunningham, M Lambros, A MacKay, C Yao, J Reis-Filho, JM. Bartlett, Molecular characterisation of isogenic taxane resistant cell lines identify novel drivers of drug resistance, BMC Cancer 14 (2014) 762, https://doi.org/10.1186/1471-2407-14-762.

[17] K Roarty, GV. Echeverria, Laboratory models for investigating breast cancer therapy resistance and metastasis, Front. Oncol. 11 (2021), 645698, https://doi.org/10.3389/fonc.2021.645698.

[18] M Winter, S Meignan, P Völkel, PO Angrand, V Chopin, N Bidan, RA Toillon, E Adriaenssens, C Lagadec, X Le Bourhis, Vimentin promotes the aggressiveness of triple negative breast cancer cells surviving chemotherapeutic treatment, Cells 10 (6) (2021) 1504, https://doi.org/10.3390/cells10061504.

[19] S Zheng, W Wang, J Aldahdooh, A Malyutina, T Shadbahr, Z Tanoli, A Pessia, J. Tang, SynergyFinder Plus: toward better interpretation and annotation of drug combination screening datasets, Genomics Proteomics Bioinformatics 20 (3) (2022) 587–596, https://doi.org/10.1016/j.gpb.2022.01.004.

[20] Q Fovez, W Laine, L Goursaud, C Berthon, N Germain, C Degand, JE Sarry, B Quesnel, P Marchetti, J. Kluza, Clinically relevant oxygraphic assay to assess mitochondrial energy metabolism in acute myeloid leukemia patients, Cancers (Basel) 13 (24) (2021) 6353, https://doi.org/10.3390/cancers13246353.

[21] C Palmieri, J Krell, CR James, C Harper-Wynne, V Misra, S Cleator, D. Miles, Rechallenging with anthracyclines and taxanes in metastatic breast cancer, Nat. Rev. Clin. Oncol. 7 (10) (2010) 561–574, https://doi.org/10.1038/nrclinonc.2010.122.

[22] E Dhimolea, R de Matos Simoes, D Kansara, A Al'Khafaji, J Bouyssou, X Weng, S Sharma, J Raja, P Awate, R Shirasaki, H Tang, BJ Glassner, Z Liu, D Gao, J Bryan, S Bender, J Roth, M Scheffer, R Jeselsohn, NS Gray, I Georgakoudi, F Vazquez, A Tsherniak, Y Chen, A Welm, C Duy, A Melnick, B Bartholdy, M Brown, AC Culhane, CS Mitsiades, An embryonic diapause-like adaptation with suppressed myc activity enables tumor treatment persistence, Cancer Cell 39 (2) (2021) 240–256, https://doi.org/10.1016/j.ccell.2020.12.002.

[23] C Bellio, M Emperador, P Castellano, A Gris-Oliver, F Canals, A Sánchez-Pla, E Zamora, J Arribas, C Saura, V Serra, J Tabernero, BA Littlefield, J. Villanueva, GDF15 Is an eribulin response biomarker also required for survival of DTP breast cancer cells, Cancers (Basel) 14 (10) (2022) 2562, https://doi.org/10.3390/cancers14102562.

[24] E Allen, P Miéville, CM Warren, S Saghafinia, L Li, MW Peng, D. Hanahan, Metabolic symbiosis enables adaptive resistance to anti-angiogenic therapy that is dependent on mTOR signaling, Cell Rep. 15 (6) (2016) 1144–1160, https://doi.org/10.1016/j.celrep.2016.04.029.

[25] ED Sunassee, BV Jardim-Perassi, MC Madonna, B Ordway, N. Ramanujam, Metabolic imaging as a tool to characterize chemoresistance and guide therapy in Triple-Negative Breast Cancer (TNBC), Mol. Cancer Res. (2023), https://doi.org/10.1158/1541-7786.MCR-22-1004. MCR-22-1004.

[26] P Marchetti, Q Fovez, N Germain, R Khamari, J. Kluza, Mitochondrial spare respiratory capacity: mechanisms, regulation, and significance in non-transformed and cancer cells, FASEB J. 34 (10) (2020) 13106–13124, https://doi.org/10.1096/fj.202000767R.

[27] KW Evans, E Yuca, SS Scott, M Zhao, N Paez Arango, CX Cruz Pico, T Saridogan, M Shariati, CA Class, CA Bristow, CP Vellano, X Zheng, AM Gonzalez-Angulo, X Su, C Tapia, K Chen, A Akcakanat, B Lim, D Tripathy, TA Yap, MED Francesco, GF Draetta, P Jones, TP Heffernan, JR Marszalek, F Meric-Bernstam, Oxidative phosphorylation is a metabolic vulnerability in chemotherapy-resistant triple-negative breast cancer, Cancer Res. 81 (21) (2021) 5572–5581, https://doi.org/10.1158/0008-5472.CAN-20-3242.

[28] Y Gong, P Ji, YS Yang, S Xie, TJ Yu, Y Xiao, ML Jin, D Ma, LW Guo, YC Pei, WJ Chai, DQ Li, F Bai, F Bertucci, X Hu, YZ Jiang, ZM Shao, Metabolic-pathway-based subtyping of triple-negative breast cancer reveals potential therapeutic targets, Cell Metab. 33 (1) (2021) 51–64, https://doi.org/10.1016/j.cmet.2020.10.012.

[29] S McGuirk, Y Audet-Delage, MG Annis, Y Xue, M Vernier, K Zhao, C St-Louis, L Minarrieta, DA Patten, G Morin, CM Greenwood, V Giguère, S Huang, PM Siegel, J. St-Pierre, Resistance to different anthracycline chemotherapeutics elicits distinct and actionable primary metabolic dependencies in breast cancer, Elife. 10 (2021) e65150, https://doi.org/10.7554/eLife.65150.

[30] ML Baek, J Lee, KE Pendleton, MJ Berner, EB Goff, L Tan, SA Martinez, I Mahmud, T Wang, MD Meyer, B Lim, JP Barrish, W Porter, PL Lorenzi, GV Echeverria, Mitochondrial structure and function adaptation in residual triple negative breast cancer cells surviving chemotherapy treatment, Oncogene 42 (14) (2023) 1117–1131, https://doi.org/10.1038/s41388-023-02596-8.